Numerical Simulation of Residual Stress in Multipass Welds for Stainless Steel Pipe

Kang-Yao HSU, and Long-Chyuan Kang

Institute of Nuclear Energy Research

Abstract

The aim of this paper is to present a computational procedure for analyzing temperature fields and residual stress states in multi-pass welds in SS304 stainless steel pipe. By using ABAQUS software, uncoupled thermal- mechanical three-dimensional finite element models are developed. The finite element models are employed to evaluate the transient temperature and the residual stress fields during welding. Through comparing the simulation results and the experimental measurements, the finite element model can be used to simulate the thermal cycles and the welding residual stresses for SS304 stainless steel pipe. The results of model are in very good with the experimental measurements.

Keywords: Multi-pass welds; Stainless Steel Pipe; Welding residual stress

1. INTRODUCTION

Residual stresses in a structural material or component are those stresses that exist in the object without (and usually prior to) the application of any service or other external loads. Manufacturing processes are the most common causes of residual stress. Virtually all manufacturing and fabricating processes - casting, welding, machining, molding, heat treatment, etc. - introduce residual stresses into the manufactured object. Another common cause of residual stress is in-service repair or modification. In some instances, stress may also be induced later in the life of the structure by installation or assembly procedures, by occasional overloads, by ground settlement effects on underground structures, or by dead loads which may ultimately become an integral part of the structure.

The circumferential butt-weld is a common type of joint in stainless steel piping systems in nuclear power plant. Owing to the relatively large wall thickness in such piping systems, the butt-weld is often constructed of several weld passes. Owing to the intense concentration of heat in the welding, the regions near the weld line undergo sever thermal cycles. The thermal cycles cause non-uniform heating and cooling in the material, thus generating inhomogeneous plastic deformation and residual stresses in the weldment. The presence of residual stresses can be detrimental to the performance of the welded product. Tensile residual stresses are generally detrimental, increasing the susceptibility of a weld to fatigue damage, stress corrosion cracking and fracture [1]. When assessing the risk for growth of defects such as surface flaws in piping systems the welding residual stress may give a large contribution to the total stress field than stress caused by design loads [2]. Moreover, in order to prevent inter-granular stress corrosion cracking in the root area of welds in stainless steel, it is necessary to satisfy certain requirements concerning process condition, material properties and welding residual stress. Therefore, a good estimation of the welding residual stress field is then needed. The distribution of welding residual stress depends on several main factors such as structural dimensions, material properties, restraint conditions, heat input, number of weld pass and welding sequence. Hence, for multi-pass welding the welding residual stresses may be very complex, and it is very difficult to predict the distribution of welding residual stress due to the multi-pass welding operation.

Over the last decade or so, a number of finite element models [1-3,5-10] have been proposed to predict temperature fields and residual stresses in multi-pass butt-welded steel pipe. Brickstad and Josefson [2] employed two-dimensional axisymmetric models to numerically simulate a series of multi-pass circumferential butt-welds of stainless steel pipe up to 40 mm thick in a non-linear thermomechanical finite element analysis. Mochizuki et al. [6] used inherent strain analysis and thermal elastic plastic analysis to predict residual stress in carbon steel pipe, and they verified their numerical models using neutron diffraction measurement. Wen et al. [7] also used a two-dimensional axisymmetric finite element model to simulate three-pass pipe girth welding with wall-thickness of 19 mm. Tsai et al. [8] employed a three-dimensional shell element and moving welding arc to simulate welding residual stress in AISI 304 stainless pipe. Li et al. [9] developed a full three-dimensional FE model to simulate a multi-pass, narrow gap girth welding process, and their research

suggested that more experimental residual stress measurements on pipe weldments are needed to verify the numerical model. Recently, Jiang and co-workers [10] used a three-dimensional FE model to predict temperature distributions in a multi-pass welded piping branch junction. However, welding residual stresses was not conducted in their research.

The past studies suggest that it is necessary to continue to carry out experiments to verify the numerical models for multi-pass butt-welded steel pipe. Three-Dimensional model can capture temperature fields and residual stress distribution in details during multi-pass welding process, however, a very long time is required because the mechanical phenomena in welding are strong non-linear transient problems. In this study, one will use ABAQUS software, a three-dimensional model was developed to simulate the temperature fields and the welding residual stress fields in SS304 stainless steel pipe to compare the experimental data conducted by Dean D. et al. [11]

2. EXPERIMENT DISCRIPTION

The material used in this work is SS304 pipe with outer diameter of 114.3 mm, thickness of 6 mm, and length of 800 mm. The welding pipe and the shape of groove are schematically shown in Fig. 1. The filler metal is ER-308L. Gas tungsten arc (GTA) welding process is used in the experiments. Welding condition is shown in Table 1. The pipe was welded by two pass welding. The inter-pass temperature is approximately 50℃. The welding direction is shown in Fig. 2 by the arrow. Welding started at circumferential angle θ= 0°, and ended at the same location.

Table 1 Welding condition

Pass	Current (A)	Voltage (V)	Speed (mm/min)	Net Het input (KJ/mm)
1	140	9.5	80	0.7
2	160	9.5	80	0.77

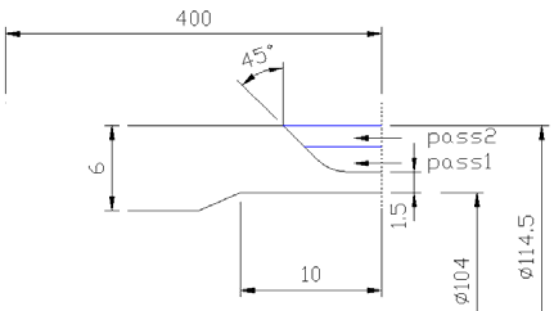

Fig. 1. Dimensions of welded pipe and shape of groove.

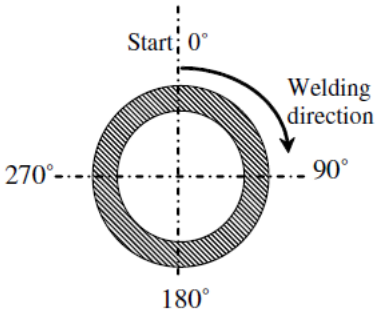

Fig. 2. Welding direction.

3. FINITE ELEMENT MODELING

The temperature fields and the evolution of the residual stresses are investigated by means of finite element method. In order to accurately capture the temperature fields and the residual stresses in the welded pipe, a 3-D finite element model is developed. The thermo-mechanical behavior of the weldment during welding is simulated using uncoupled formulation, because the dimensional changes in welding are negligible and mechanical work done is insignificant compared to the thermal energy from the welding arc.

The heat conduction problem is solved independently from the stress problem to obtain temperature history. However, the formulation considers the contributions of the transient temperature field to the stress analysis through thermal expansion, as well as temperature-dependent thermo-physical and mechanical properties. The solution procedure consists of two steps. First, the temperature distribution and its history in the welding model is computed by the heat conduction analysis. Then, the temperature history is employed as a thermal load in the subsequent mechanical elastic plastic calculation of the residual stress field.

In this study, all analyses are performed using ABAQUS code. The base metal and weld metal are defined as different materials. The thermal physical properties and mechanical properties of the base metal are shown in Table 2. For the weld metal, only the yield stress is higher than that of the base metal, the other properties are almost the same as the base metal.

Table 2 Thermal physical properties and mechanical properties of SUS304

T (℃)	Spec. heat (J/kg℃)	Cond (J/mm ℃s)	Density (kg/m^3)	Yield stress (MPa)	Th. exp ($\times 10^{-6}$ $℃^{-1}$)	E (GPa)	ν
0	462	0.0146	7900	265	17.0	198.5	0.294
100	496	0.0151	7880	218	17.4	193	0.295
200	512	0.0161	7830	186	18.0	185	0.301
300	525	0.0179	7790	170	18.6	176	0.310
400	540	0.0180	7750	155	19.1	167	0.318
600	577	0.0208	7660	149	19.6	159	0.326
800	604	0.0239	7560	91	20.2	151	0.333
1200	676	0.0322	7370	25	20.7	60	0.339
1300	692	0.0337	7320	21	21.1	20	0.342
1500	700	0.1200	7320	10	21.6	1	0.388

3.1. Thermal Analysis

The 3-D finite element model is shown in Fig. 3 with 12310 brick elements and 18916 nodes. Because of the symmetry, only one half of the model is selected as the analysis model. It has a fine grid in the welding zone. During the thermal analysis the model change option is used to simulate the weld metal deposition. During the first weld pass, the second weld pass does not exist in the model. After the completion of the first welding, new elements are added to the model to simulate the weld metal deposition into the groove during the second welding.

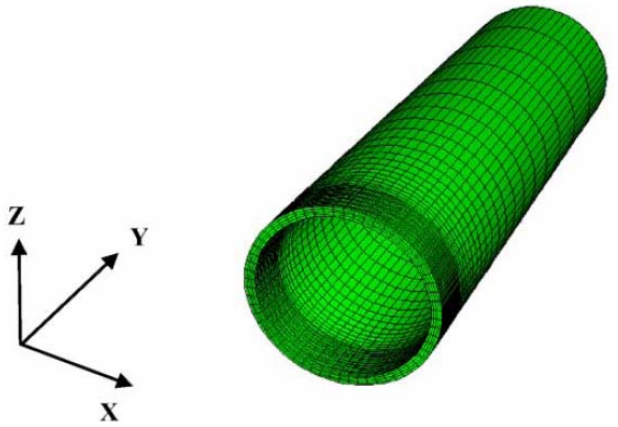

Fig. 3. Three-Dimensional finite element model.

In thermal analysis, the governing equation for transient heat transfer analysis is given by

$$\rho c \frac{\partial T}{\partial t}(x,y,z,t) = -\nabla \cdot \vec{q}(x,y,z,t) + Q(x,y,z,t) \quad (1)$$

where ρ is the density of the materials, c is the specific heat capacity, T is the current temperature, $\vec{q}$ is the heat flux vector, Q is the internal heat generation rate, x, y and z are the global coordinates in the reference system, t is the time, and ∇ is the spatial gradient operator.

The non-liner isotropic Fourier heat flux constitutive equation is employed:

$$q = -k.\nabla T \quad (2)$$

where k is the temperature-dependent thermal conductivity.

In this study, the heat from the moving welding arc is applied as a volumetric heat source with a double ellipsoidal distribution proposed by Goldak et al. [3], and is expressed by the following equations:

$$Q(x,y,z,t) = \frac{6\sqrt{3} f_f Q_w}{a_1 bc\pi\sqrt{\pi}} \exp\left(-\frac{3x^2}{a_1^2}\right)\exp\left(-\frac{3y^2}{b^2}\right)\exp\left(-\frac{3z^2}{c^2}\right) \quad (3)$$

For the front heat source:

$$Q(x,y,z,t) = \frac{6\sqrt{3} f_r Q_w}{a_1 bc\pi\sqrt{\pi}} \exp\left(-\frac{3x^2}{a_2^2}\right)\exp\left(-\frac{3y^2}{b^2}\right)\exp\left(-\frac{3z^2}{c^2}\right) \quad (4)$$

where x, y and z are the local coordinates of the double ellipsoid model aligned with the welded pipe; f_f and f_r are parameters which give the fraction of the heat deposited in the front and the rear parts, respectively. Note that $f_f + f_r = 2.0$. In this study, f_f is assumed to be 1.4 and f_r 0.6. This is done because the temperature gradient in the front leading part is steeper than in the tailing edge [4].

Q_w is the power of the welding heat source. It can be calculated according to the welding current, the arc voltage and the arc efficiency. The welding efficiency is assumed to be 70% for the TIG welding process. The parameters a_1, a_2, b and c are related to the characteristics of the welding heat source. The parameters of the heat source can be adjusted to create a desired melted zone according to the welding conditions. The moving heat source is modeled by a user subroutine in ABAQUS code.

In order to consider the heat losses, both the thermal radiation and heat transfer on the weld surface are assumed. Radiation losses are dominating for higher temperatures near and in the weld zone, and convection losses for lower temperatures away from the weld zone. A user subroutine was developed to simulate the combined thermal boundary condition. The total temperature-dependent heat transfer coefficient h (W/mm^2) is given as below [2].

$$\begin{aligned} h &= 0.68\ T\times10^{-8} && \text{for } 0 < T < 500℃ \\ h &= 0.231\ T\text{-}82.1)\times10^{-6} && \text{for } T > 500℃ \end{aligned} \quad (5)$$

where T is the temperature.

The above thermal boundary condition is employed for all free boundaries of the 3-D pipe including the boundaries generated by the second weld pass. To account for heat transfer due to fluid flow in the weld pool, an artificially increased thermal conductivity, which is several times larger than the value at room temperature, is assumed for temperatures above the melting point. The thermal effects due to solidification of the weld pool are modeled by taking into account the latent heat of fusion.

3.2. Mechanical Analysis

The same finite element model used in the thermal analysis was employed in mechanical analysis except for the element type and the boundary conditions. The mechanical analysis is conducted using the temperature histories computed by the thermal analysis as the input data. In the duration of welding, because solid-state phase transformation does not occur in the stainless base metal and the weld metal, the total strain rate can be decomposed into three components as follows:

$$\dot{\varepsilon} = \dot{\varepsilon}^e + \dot{\varepsilon}^p + \dot{\varepsilon}^{th} \quad (6)$$

The components on the right hand side of Eq. (6) correspond to elastic strain, plastic strain and thermal strain, respectively. The elastic strain is modeled using the

isotropic Hook's law with temperature-dependent Young's modulus and Poissons ratio as shown in Table 2. The thermal strain is computed using the temperature-dependent coefficient of thermal expansion. For the plastic strain, a rate-independent plastic model is employed with the following features: the Von Mises yield surface, temperature-dependent mechanical properties, and linear kinematic hardening model. Kinematic hardening is taken into account an important feature because material points typically undergo both loading and unloading in course of the welding process [5].

4. SIMULATED RESULTS

4.1. Simulated Results of Thermal Analysis

The temperature field during the welding is shown in Fig. 4. From this figure, it can be observed that the maximum temperature in the weld pool is 2200℃ or so. This result agrees with the welding process in practice.

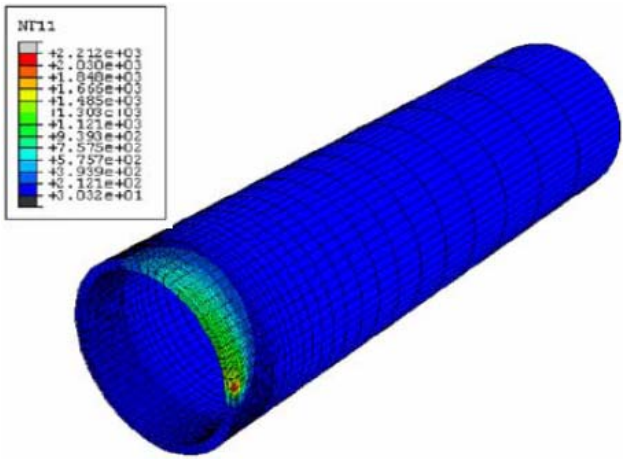

Fig. 4. Welding temperature field distribution

Fig. 5 shows the thermal cycles during the first welding at three locations where circumferential angle θ is 180° on the inside surface and the outside surface. Fig. 6 shows the thermal cycles at three locations on the outside surface. From this figure, we can observe that both the peak temperature and the cooling rate at each location are in very good agreement with the experimental measurements.

The thermal cycles at different circumferential locations on the inside surface during the first welding are plotted in Fig. 7. The curves with solid marks represent the temperature histories at those locations where θ is 90° on the inside surface, the broken curves the temperature histories at those locations where θ is 180°, and curves without any mark the temperature histories at those locations where θ is 270°. From this figure, it is very clear that the temperature histories at the three locations on the surface where θ is 90° are almost identical to those at the corresponding three locations on the surface where θ is 180℃ or 270°. Therefore, it can be concluded that the temperature filed is very steady when the welding torch moving around the pipe. The reason can be considered that comparing with the welding speed the heat conduction rate is much small because of a relatively small conductivity.

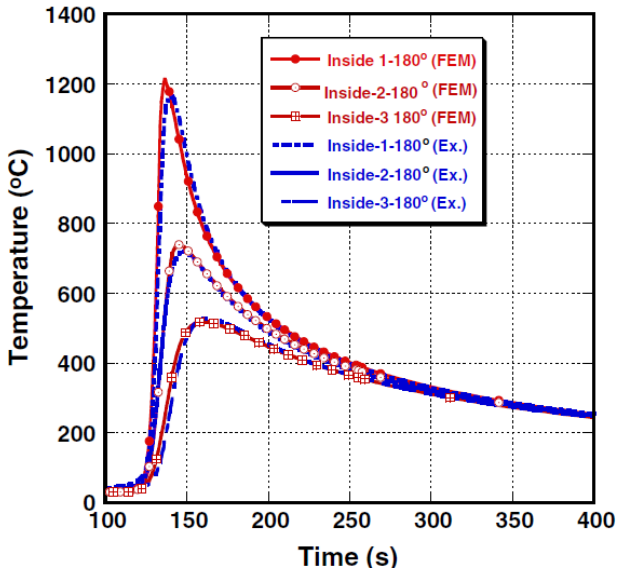

Fig. 5. Thermal cycles at three locations on the inside surface after the first welding.

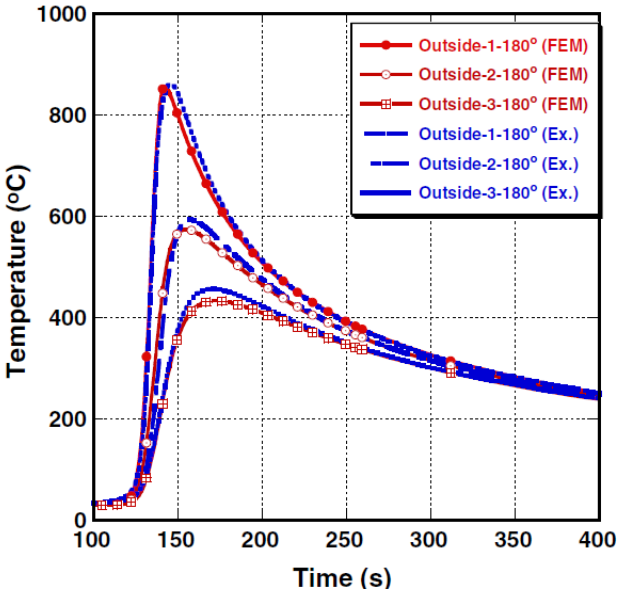

Fig. 6. Thermal cycles at three locations on the outside surface after the first welding.

4.2. Simulated Results of Mechanical Analysis

Fig. 8 shows the axial stress of the welded pipe. Through careful observation of this figure, it can be found that the axial stresses at the start of welding and its vicinity are slightly different from the other locations. Except for this part, the axial stress around

the circumferential direction almost has a homogeneous distribution.

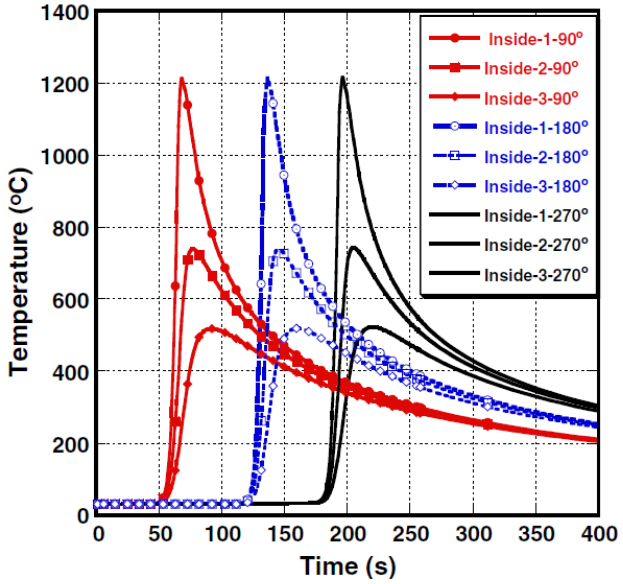

Fig. 7. Thermal cycles at several locations on the inside surface during the first welding.

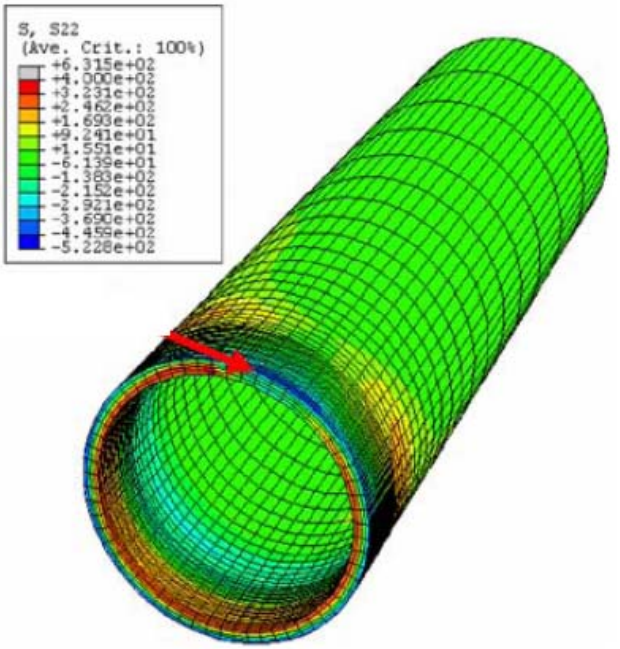

Fig. 8. Axial stress distributions of the welded pipe.

Figs. 9 and 10 show the axial stresses and the hoop stresses at locations with different angle θ, respectively. In Fig. 9, the axial stress distribution seems not to be sensitive to the angle θ. In Fig. 10, when θ is 0° the hoop stress distribution in weld zone and its vicinity is slightly different from that of other three locations (θ = 90°, 180° and 270°) because of the end effect. When θ is 90° the hoop stress at locations Y = 30 mm is the smaller than that of the other three locations (θ = 0°, 180° and 270°). However, in general, both the axial stress and the hoop stress are not significantly sensitive to the angle θ. It means that the stress distribution around the circumferential direction can be regarded as homogeneous distribution.

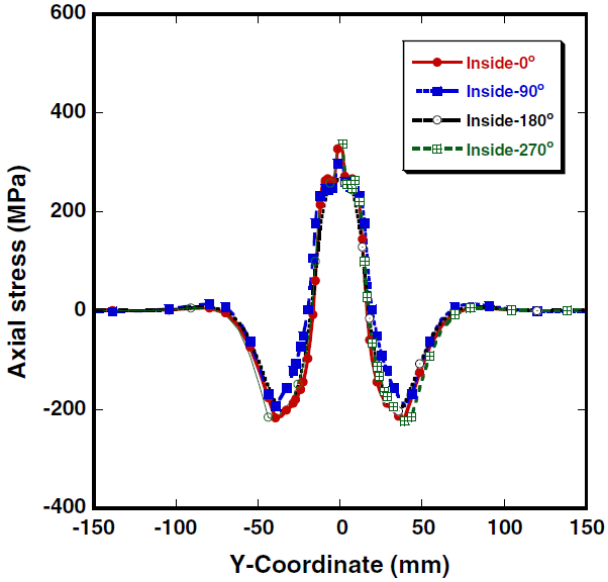

Fig. 9. Axial stress distributions on the inside surface.

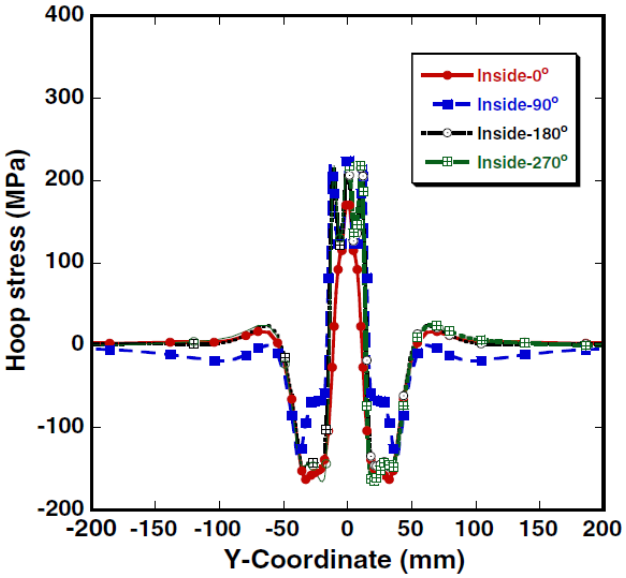

Fig. 10. Hoop stress distribution on the inside surface.

5. COMPARISON WITH EXPERIMENTAL MEASUREMENTS

The residual stresses at the locations along the axial direction, in which the angle θ is 180°, are selected to compare with the experimental measurements. Figs. 11 and 12 show the axial stress and the hoop stress on the inside surface along the axial direction, respectively. The black spots represent the results of the experimental value measured by strain gauges, the solid curves the results of the 3-D model. In the two figures, the simulated results are in very good agreement with the experimental

measurements. In the weld zone, because of high yield strength of the weld metal, the final welding residual axial stress is much large. In Fig. 11, both the numerical results and the experimental measurements reflect this feature.

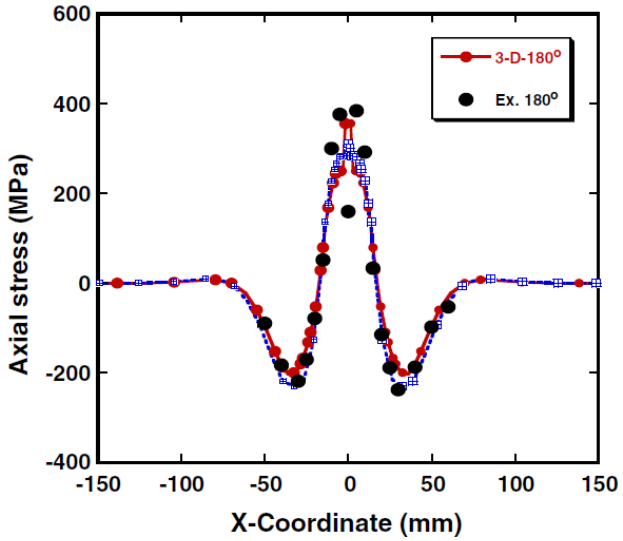

Fig. 11. Axial stress distribution on the inside surface.

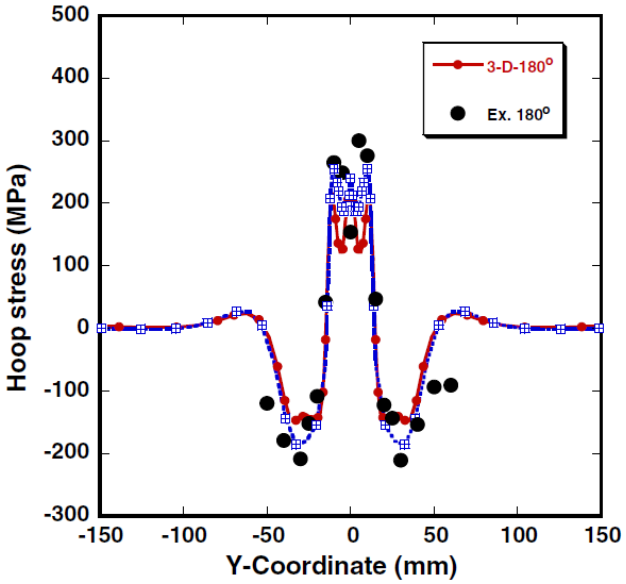

Fig. 12. Hoop stress distribution on the inside surface.

Figs. 13 and 14 show the axial stress and the hoop stress on the outside surface along the axial direction, respectively. From Fig. 13, it is clear that the axial stresses are in very good agreement with the experimental measurements. At the weld zone and its vicinity, the hoop stress distribution measured by experiment is also similar to the simulation results. However, within the range where the distance from the weld centerline is larger than 40 mm, the hoop stresses measured by strain gauges are much larger than the simulation results. This difference is caused by the initial residual stress introduced by the manufacturing process before welding. Because the weld zone and its vicinity experienced very high temperature histories during welding, plastic strains were generated in this part. The initial residual stresses have no influence on the final welding residual stress. In contrast, in the parts which are away from the weld zone, the initial residual stresses are nearly not affected by welding. In Fig. 14, it can be seen that the initial residual stresses remain the place where the distance from the weld centerline is larger than 40 mm.

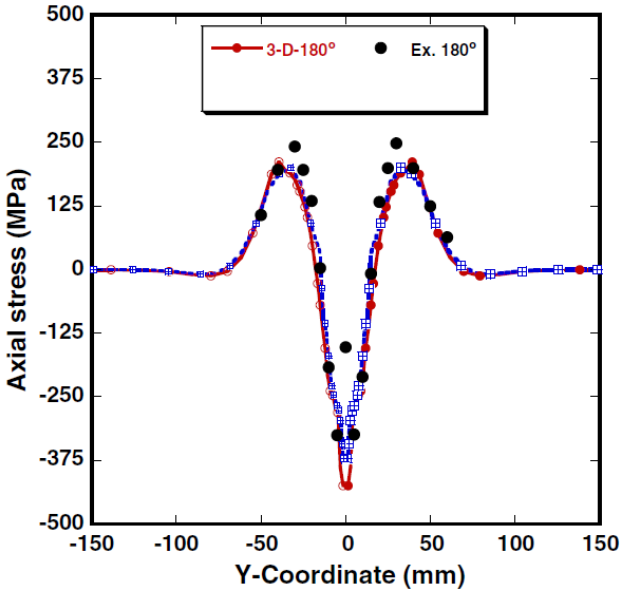

Fig. 13. Axial stress distribution on the outside surface.

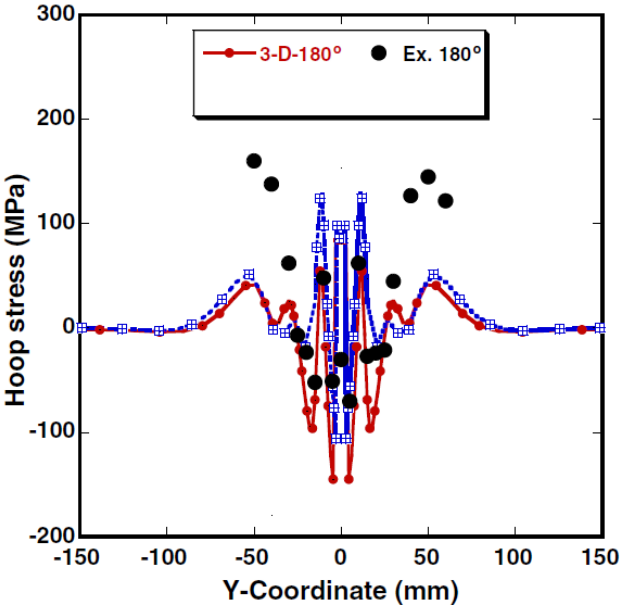

Fig. 14. Hoop stress distribution on the outside surface.

According to the comparisons and the discussions, we can conclude that ABAQUS model can be used to simulate the temperature fields and the welding residual stress fields for SS304 stainless steel pipe. Based on the results of the residual stress, the characteristics of welding residual stress distribution in the stainless pipe used in this study can be described as follows. Because the thickness of the pipe is 6 mm, the inside surface near the weld zone

can reach a very high temperature (>1000℃) when the outside is welded. Thus, the plastic deformation is prone to produce in the whole cross-section in the weld zone and its vicinity during the second welding.

During the cooling, because the weld zone and its vicinity shrink, the diameters in this part become smaller, and a bending moment is generated due to the deformation. Therefore, a tensile axial stress is produced on the inside surface, and compressive axial stress on the outside surface. The magnitude of the maximum axial stresses in both the inside surface and the outside surface reach the yield stress at room temperature. Tensile axial stresses are formed on the outside surface away from the weld centerline, and compressive axial stresses on the inside surface. On the inside surface, the shape of hoop stress is very similar to the axial stress. At the weld zone and its vicinity tensile hoop stresses are generated, and compressive stresses are produced away from the weld centerline. The distribution of the hoop stress on the outside surface is very complex. Observing the simulation results and experiment, it can be found that the shape is like a wave and very sensitive to the distance from the weld centerline.

6. CONCLUSIONS

In this study, ABAQUS finite element model was developed to analyze the temperature fields and the residual stress distributions for SS304 stainless steel pipe. By comparisons with the experimental measurements, it has been proved that the ABAQUS computational model can be used for predicting the thermal cycles and the welding residual stresses. According to the simulated and experimental results, one can draw the following conclusions:

(1) Based on the simulated results, it is clear that the temperature distribution around the heat source is very steady when the welding torch moves around the stainless steel pipe. From simulated results, it can be also seen that the residual stress around the circumferential direction almost has a homogenous distribution except for the welding start part.

(2) The distribution characteristics of residual stress distributions in the stainless steel pipe can be described as follows. The axial residual stresses on the insider surface and the outside surface have a contrary distribution. In weld zone and its vicinity, a tensile axial residual stress is produced on the inside surface, and compressive axial stress at outside surface. Away from the weld centerline, tensile axial stress is formed on the outside surface, and compressive axial stress on the inside surface. On the inside surface, the shape of hoop stress distribution is very similar to the axial stress. The shape of the hoop stress distribution on the outside surface is very sensitive to the distance from the weld centerline.

7. REFERENCES

[1] S. Murugan, S.K. Rai, P.V. Kumar, T. Jayakumar, Baldev Raj, M.S.C. Bose, International Journal of Pressure Vessels and Piping 78 (2001) 307–317.

[2] B. Brickstad, B.L. Josefson, International Journal of Pressure Vessels and Piping 75 (1998) 11–25.

[3] J. Goldak, A. Chakravarti, M. Bibby, Metallurgical Transactions B 15 (June) (1984) 299–305.

[4] D. Deng, Y. Luo, H. Serizawa, M. Shibahara, H. Murakawa, JWRI 32 (2) (2003) 325–333.

[5] D. Radaj, Welding Residual Stresses and Distortion Calculation and Measurement—DVS, Verlag, 2003, ISBN 3-87155-791-9.

[6] M. Mochizuki, M. Hayashi, T. Hattori, Journal of Engineering Materials and Technology 122 (January) (2000) 98–103.

[7] S.W. Wen, P. Hilton, D.C.J. Farrugia, Strain Journal of the British Society for Strain Measurement 37 (1) (2001) 15–18.

[8] C.L. Tsai, Y. Dong, P. Dong, 77th Annual AWS, Chicago, USA, 21–25 April 1996, p. 51.

[9] M. Li, D.G. Atteridge, L.L. Meekisho, S.L. West, Trends in Welding Research, 4th International Conference, Gaylingurg, Tennessee, USA, 5–8 June 1995, pp. 51–56.

[10] W. Jiang, K. Yahiaoui, F.R. Hall, Journal of Pressure Vessel Technology 127 (February) (2005) 7–12.

[11] Dean D., Hidekazu M., Numerical simulation of temperature field and residual stress in multi-pass welds in stainless steel pipe and comparison with experimental measurements, Computational Materials Science 37 (2006) 269–277.